Published in final edited form as:

Neuroscience. 2015 October 29; 307: 83–97. doi:10.1016/j.neuroscience.2015.08.029.

Sex differences in NMDA GluN1 Plasticity in Rostral Ventrolateral Medulla Neurons Containing Corticotropin Releasing Factor Type 1 Receptor following Slow-Pressor Angiotensin II Hypertension

Tracey A. Van Kempen[1,2], **Mariana Dodos**[1], **Clara Woods**[1], **Jose Marques-Lopes**[1], **Nicholas J. Justice**[4], **Costantino Iadecola**[1,2], **Virginia M. Pickel**[1,2], **Michael J. Glass**[1,2,*], and **Teresa A. Milner**[1,2,3,*]

[1]Feil Family Brain and Mind Research Institute, Weill Cornell Medical College, 407 East 61st Street, New York, NY 10065

[2]Weill Cornell Graduate School of Medical Sciences, Weill Cornell Medical College, 1300 York Ave, New York, NY 10021

[3]Harold and Margaret Milliken Hatch Laboratory of Neuroendocrinology, The Rockefeller University, 1230 York Avenue, New York, NY 10065

[4]Institute of Molecular Medicine, The University of Texas Health Science Center at Houston, 1825 Pressler St., Houston Texas 77030

Abstract

There are profound, yet incompletely understood, sex differences in the neurogenic regulation of blood pressure. Both corticotrophin signaling and glutamate receptor plasticity, which differ between males and females, are known to play important roles in the neural regulation of blood pressure. However, the relationship between hypertension and glutamate plasticity in corticotrophin-releasing hormone (CRF) receptive neurons in brain cardiovascular regulatory areas, including the rostral ventrolateral medulla (RVLM) and paraventricular nucleus of the hypothalamus (PVN), is not understood. In the present study, we used dual label immunoelectron microscopy to analyze sex differences in slow-pressor angiotensin II (AngII) hypertension with respect to the subcellular distribution of the obligatory GluN1 subunit of the N-methyl-D-aspartate receptor (NMDAR) in the RVLM and PVN. Studies were conducted in mice expressing the

Address correspondence to: Dr. Teresa A. Milner or Dr. Michael. J. Glass, Feil Family Brain and Mind Research Institute, Weill Cornell Medical College, 407 East 61st Street, New York, NY 10065, Phone: 646-962-8274 (TAM); 646-962-8253 (MJG), FAX: 646-962-0535, tmilner@med.cornell.edu; mjg2003@med.cornell.edu.
*Co-senior authors

Conflict of Interest: The authors declare no competing financial interests.

Author contributions. TAVK: designed studies, collected data, data analysis, wrote manuscript; MD, CW: data collection and analysis; JM-L: prepared animals, wrote manuscript; NJJ: provided animals, wrote manuscript; CI, VMP: grant support, wrote manuscipt; MJG: designed studies, wrote manuscript, grant support, supervised CW; TAM: grant support, designed studies, prepared brains specimens, data collection, wrote manuscript

enhanced green fluorescence protein (EGFP) under the control of the CRF type 1 receptor (CRF_1) promoter (i.e., CRF_1-EGFP reporter mice). By light microscopy, GluN1-immunoreactivity was found in CRF_1-EGFP neurons of the RVLM and PVN. Moreover, in both regions tyrosine hydroxylase was found in CRF_1-EGFP neurons. In response to AngII, male mice showed an elevation in blood pressure that was associated with an increase in the proportion of GluN1 on presumably functional areas of the plasma membrane in CRF_1-EGFP dendritic profiles in the RVLM. In female mice, AngII was neither associated with an increase in blood pressure nor an increase in plasma membrane GluN1 in the RVLM. Unlike the RVLM, AngII-mediated hypertension had no effect on GluN1 localization in CRF_1-EGFP dendrites in the PVN of either male or female mice. These studies provide an anatomical mechanism for sex-differences in the convergent modulation of RVLM catecholaminergic neurons by CRF and glutamate. Moreover, these results suggest that sexual dimorphism in AngII-induced hypertension is reflected by NMDA receptor trafficking in presumptive sympathoexcitatory neurons in the RVLM.

Graphical Abstract

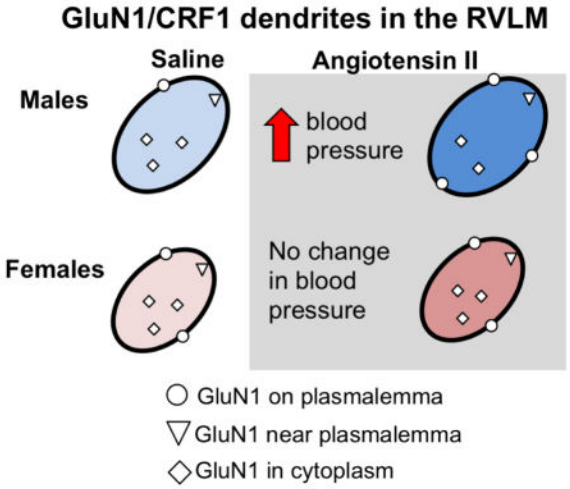

Keywords

paraventricular nucleus of the hypothalamus; C1 catecholaminergic neurons; catecholamine; sympathoexcitatory neurons; hypertension; electron microscopy

Stress is a significant risk factor for cardiovascular disease (Cohen et al., 2015; Dimsdale, 2008). Hypertension (Cheng et al., 2012; Hart and Charkoudian, 2014; Xue et al., 2007b) and stress responses (Goel et al., 2014; McEwen, 2010; Wang et al., 2007) also are known to substantially differ in males and females. Elucidating the neurobiological substrates of these differences could contribute to developing gender-specific treatments for hypertension and stress-related disorders (Appelman et al., 2015; Prata et al., 2014).

The neural control of blood pressure involves sympathoexcitatory outflow that is critically regulated by neurons of the rostral ventrolateral medulla (RVLM) (Chan and Chan, 2014; Nunn et al., 2011). Glutamate plays an important role in regulating sympathetic outflow from the RVLM via neurons projecting to the intermediolateral nucleus of the spinal cord

(Chan and Chan, 2014). Microinjection of N-methyl-D-aspartate (NMDA) in the RVLM results in a pressor response in normal animals (Kagiyama et al., 2001; Takemoto, 2007) and spontaneously hypertensive rats show an exaggerated pressor response to RVLM NMDA administration (Lin et al., 2005). In addition, RVLM NMDA receptors have been shown to play an important role in the pressor response following carotid body chemoreceptor stimulation (Kubo et al., 1993) and muscle contraction (Reidman et al., 2000), as well as in the elevated blood pressure seen in rats with chronic heart failure (Wang et al., 2009) and in spontaneously hypertensive rats (Lin et al., 1995; Lin et al., 2005; Zhang and Abdel-Rahman, 2002).

The obligatory GluN1 subunit of the heteromeric, ionotropic NMDA receptor (Dingledine et al., 1999) is expressed in the RVLM (Llewellyn-Smith and Mueller, 2013).. Activity-dependent changes in the subcellular localization of GluN1 are a critical component of neural plasticity in a variety of brain regions (Beckerman et al., 2013; Petralia, 2012). Several studies in male mice demonstrate that increased blood pressure is associated with alteration of the subcellular localization of GluN1 in brain areas involved in sympathoexcitatory outflow, including hypothalamic paraventricular nucleus (PVN) neurons (Coleman et al., 2010; Glass et al., 2015; Marques-Lopes et al., 2014; Wang et al., 2013). Little is known, however, about the relationship between hypertension and GluN1 trafficking in the RVLM.

Stress can influence blood pressure (Busnardo et al., 2013) and may contribute to hypertension (Cuffee et al., 2014). Corticotropin releasing factor (CRF) and its type 1 receptor (CRF_1) in the PVN and other brain areas have long been associated with both stress responses and with homeostatic regulation (Goncharuk et al., 2002; Ku et al., 1998; Smith et al., 1998). In male rats, CRF acts in the RVLM and PVN to increase systemic arterial pressure (Ku et al., 1998; Milner et al., 1993). Thus, in both the RVLM and PVN, neurons expressing CRF_1 may play a role in regulating blood pressure in response to stress.

There are sex differences in the emergence of both hypertension and hypothalamic plasticity. In young male mice, slow-pressor AngII administration results in a slow-onset increase in arterial pressure that develops over several days (Kawada et al., 2002; Zimmerman et al., 2004; Reckelhoff and Romero, 2003). However, young aged-matched female mice do not develop hypertension in response to slow pressor AngII (Marques-Lopes et al., 2015; Marques-Lopes et al., 2014; Xue et al., 2007a). Notably, the subcellular distribution and pattern of GluN1 in distinct populations of PVN dendrites also differs in young male and female mice following slow-pressor AngII administration (Marques-Lopes et al., 2015; Marques-Lopes et al., 2014). In particular, GluN1 is increased in estrogen receptor (ER) β-containing dendrites in hypertensive males, but decreased in non-hypertensive females (Marques-Lopes et al., 2014). However, the effect of slow-pressor AngII administration on the subcellular distribution GluN1 has not yet been explored in CRF_1 neurons in either the RVLM or PVN.

Substantial sex differences in the cellular response to CRF have been demonstrated in several brain regions (Smith et al., 1998; Valentino et al., 2013; Weathington et al., 2014). Thus, given the known involvement of GluN1 in sympathoexcitatory responses in the

RVLM and the PVN, as well as important interactions between CRF_1 and NMDA receptor-mediated signaling (Fu and Neugebauer, 2008; Sheng et al., 2008), we used dual label immunoelectron microscopy to analyze the subcellular distribution of GluN1 in both brain areas in response to slow-pressor AngII administration. This analysis was performed in young male and female bacterial artificial chromosome (BAC) transgenic mice expressing the enhanced green fluorescence protein (EGFP) under the control of the CRF_1 promoter (CRF_1-EGFP) (Justice et al., 2008).

EXPERIMENTAL PROCEDURES

Animals

Experiments were approved by the Weill Cornell Medical College Institutional Animal Care and Use Committee and conducted in accordance with the NIH Guide for the Care and Use of Laboratory Animals. Male and female adult (aged-matched; ~2–3 month old) BAC transgenic mice expressing EGFP under the control of the CRF_1 promoter (i.e., CRF_1 reporter mice) (Justice et al., 2008) were used in these experiments. The details on the characterization of this mouse have been described previously (Justice et al., 2008). Briefly, CRF_1-EGFP mice were initially developed by the GENSAT project (www.gensat.org) at The Rockefeller University (Gong et al., 2003). CRF_1-EGFP labeling extensively colocalizes with CRF_1 mRNA (Justice et al., 2008). CRF_1-EGFP mice were maintained on the C57/Bl6 background. Male and female mice were between 2 and 3 months old at the beginning of the experiment. All mice were kept on a 12:12 light/dark cycle (lights on at 6:00 AM) and housed in groups of 4–5 with *ad libitum* access to food and water. Estrous cycle stage was determined at the termination of the experiment using vaginal smear cytology (Turner and Bagnara, 1971). All female mice used in this study were in estrus (declining estrogen levels and elevated progestin levels).

Slow-pressor AngII and tail cuff plesthysmography

As previously described (Marques-Lopes et al., 2014), osmotic minipumps (Alzet, Durect Corporation, Cupertino, CA) were filled with AngII dissolved in saline solution (0.9% NaCl in 0.01% bovine serum albumin; BSA) or the saline solution alone (Sal). To determine the appropriate amount of AngII (600 ng/kg/min) mice were weighed prior to pump preparation. Pumps were incubated in saline at 37°C overnight and then implanted subcutaneously in anesthetized mice (isofluorane; 5% induction, 1.5–2% maintenance). Mice were implanted with osmotic mini-pumps for a total of 14 days. Systolic blood pressure (SBP) was measured in awake mice (N = 3/group) prior to implanting pumps and on days 2, 9–10 and 13 post-implant using tail cuff plethysmography (Model MC4000, Hatteras Instruments, Cary, NC) as previously described (Coleman et al., 2010). Tail-cuff plethysmography provides a reliable non-invasive method to compare SBP measurements between groups (Capone et al., 2012; Coleman et al., 2013; Wang et al., 2013). The limitations of using tail-cuff phethysmography have been discussed previously (Marques-Lopes et al., 2014).

Retrograde labeling of spinally projecting PVN neurons

A custom-made Hamilton syringe (model 75 SN SYR, 5 μl, 32 gauge; Reno, NV) was used to pressure inject 1 μl of 4% Fluoro-Gold (FG); Fluorochrome, Denver, CO) into the

intermediolateral region of the spinal cord (T2–T4 level) after dorsal laminectomy of anesthetized (isoflurane) adult male mice (N = 4), as previously described (Marques-Lopes et al., 2015). Injections in this region optimize retrograde transport of fluorogold to the PVN. Mice were euthanized 10 days following spinal injections and spinal and brain sections were processed for fluorescence immunohistochemistry as described below.

Antisera

The specificity of the chicken anti-GFP antisera (GFP1020, Aves Labs, San Diego, CA) has been demonstrated using immunohistochemistry and western blotting (GFP-1020 data sheet). This antibody has been used to label EGFP expression in several different transgenic mouse lines (Gonzalez et al., 2012; Marques-Lopes et al., 2015; Marques-Lopes et al., 2014; Milner et al., 2010). In addition, this antibody does not label cells in brain tissue from mice lacking EGFP (Gonzalez et al., 2012).

A monoclonal mouse antiserum (clone 54.1; BD Biosciences, San Diego, CA) was used to label the GluN1 subunit of NMDAR. The specificity of this antibody has been extensively characterized via immunoprecipitation and immunohistochemistry in mice, rats, monkeys, and transfected HEK 293 cells (Brose et al., 1994; Siegel et al., 1994; Siegel et al., 1995). It has also been verified in mice with brain site-specific GluN1 deletion (Glass et al., 2013). This antibody has been used extensively in previous publications (Beckerman et al., 2013; Glass et al., 2008; Marques-Lopes et al., 2015; Marques-Lopes et al., 2014; Wang et al., 2013).

The specificity of the guinea pig antiserum raised against Fluorogold (NM101; Protos Biotech, New York, NY) has been previously characterized in preadsorption assays (see data sheet) and has been used to identify retrogradely labeled neurons of the mouse hippocampus (Jinno and Kosaka, 2002) and PVN (Marques-Lopes et al., 2015), as well as the rat PVN (Perello and Raingo, 2013), and spinal cord (Polgar et al., 2007).

An anti-ERβ antibody raised in rabbits (Z8P; Zymed Laboratories, San Francisco, CA) was used. This antibody recognizes a peptide sequence in the C-terminus (aa 468–485) of the mouse ERβ protein (Shughrue and Merchenthaler, 2001). Specificity for ERβ has been shown by Western blot, double label with mRNA using *in situ* hybridization, preadsorption control and absence of labeling in fixed brain sections prepared from ERβ knock-out mice (Creutz and Kritzer, 2002; Shughrue and Merchenthaler, 2001).

A guinea pig polyclonal antiserum raised against arginine vasopressin (AVP; #t-5048, Peninsula Laboratories, San Carlos, CA) has been shown to recognize AVP without oxytocin cross-reactivity (Coleman et al., 2013). No immunolabeling is seen using this antiserum in Brattleboro rats, which do not express AVP (Drouyer et al., 2010).

The specificity of the sheep polyclonal antiserum against tyrosine hydroxylase (AB1542; EMD Millipore, Temecula, CA) has been previously demonstrated via western blot of okadaic acid stimulated PC12 cells (manufacturer's data sheet) and via immunohistochemistry (Gonzalez et al., 2012; Kaufling et al., 2009; Noack and Lewis, 1989).

Immunofluorescence microscopy

Adult, male (N = 9) and female (N = 3) mice were deeply anesthetized with sodium pentobarbital (150 mg/kg, I.P.) and perfused sequentially through the ascending aorta with: 1) ~5 mls 0.9% saline containing 40 units of heparin; and 2) 4% paraformaldehyde in 0.1M phosphate buffer (pH 7.4; PB). Whole brains were post-fixed in the latter fixative overnight and then transferred to PB and cut into 5mm coronal blocks using a brain mold (Activational systems). The blocks were then sectioned (40 μm thick) on a vibrating microtome (Vibratome; Leica) and collected in PB. Sections were stored in cryoprotectant (30% sucrose, 30% ethylene glycol in PB) at −20°C until immunocytochemical processing (Milner et al., 2011).

For each animal, 2–3 sections were selected from the PVN (−0.50 to −1.10 mm from Bregma) and RVLM (−6.8 to −7.2 mm from Bregma) (Hof et al., 2000). This region of the RVLM has been shown previously to harbor C1 neurons that project to the spinal cord (Guyenet et al., 2013; Phillips et al., 2001; Wang et al., 2006). Localization of ERβ was performed in female mice, whereas all other markers were localized in male mice. Sections were processed for immunofluorescence as previously described (Marques-Lopes et al., 2015; Marques-Lopes et al., 2014).

Brain sections were incubated in 0.5% BSA in PB for 30 minutes to block non-specific antisera binding. Next, sections were incubated in primary antisera (chicken anti-GFP 1:10,000; guinea pig anti-FG 1:1000; sheep anti-TH 1:2000; guinea pig anti-AVP 1:1200) for 24 hours at room temperature and then for 24 hours at 4°C. Brain sections then were incubated in secondary antibodies (1:400; Invitrogen-Molecular Probes, Carlsbad, CA) for 2 hours at room temperature (GFP: Alexa Fluor 488 goat anti-chicken IgG; FG: Cy5 donkey anti-guinea pig IgG; TH: rabbit anti-sheep IgG; AVP: Cy5 donkey anti-guinea pig IgG). After secondary antibody labeling, sections were mounted on gelatin-coated slides and coverslipped with slowFade Gold reagent (Invitrogen-Molecular Probes, Grand Island, NY). Micrographs were acquired using a Leica (Nusslock, Germany) confocal microscope. Z-stack analysis was employed to verify dually-labeled neurons. The PVN was defined by its location dorsolateral to the third ventricle and medial to the fornix. The RVLM was defined by its location between the nucleus ambiguous and ventral surface. For quantification, 4 sections across the rostro-caudal extent of the PVN and 3 sections from the RVLM were chosen to ensure that mid-level sections were available for quantification for each animal (N = 4). The number cells with only TH-labeling, GFP-labeling, and those cells showing both TH- and GFP-labeling were counted in the PVN and RVLM of each animal.

Dual label immunohistochemistry for electron microscopy

The same investigator (TAM) perfused all mice to maintain consistency between all groups. On the day of perfusion, females were in estrus (declining estrogen and high progestin) or diestrus1 (low estrogen and progestin); none of the females were in proestrus (high estrogen state). Mice (N = 3 per experimental condition) were deeply anesthetized with sodium pentobarbital (150 mg/kg, i.p.) and perfused sequentially through the ascending aorta with: 1) ~5 ml saline (0.9%) containing 2% heparin, and 2) 30 ml of 3.75% acrolein and 2% paraformaldehyde in PB (Milner et al., 2011). Following removal from the skull, the brain

was post-fixed for 30 minutes in 2% acrolein and 2% paraformaldehyde in PB. Brains were then sectioned and stored as described above.

For each animal, 2–3 PVN and RVLM sections were processed for immunoelectron microscopy (immunoEM) experiments using previously described methods (Milner et al., 2011). Prior to immunohistochemical processing, sections were rinsed in PB, and experimental groups were coded with hole-punches so that tissue could be run in single crucibles, ensuring identical exposure to all reagents (Pierce et al., 1999). For PVN sections, male and female groups were run in separate immunoEM experiments. For RVLM sections, male and female groups were run in a single immunoEM experiment.

Prior to processing for dual immunolabeling, sections were treated with 1% sodium borohydride for 30 minutes to remove free aldehyde sites. Sections then were rinsed in PB followed by a rinse in 0.1 M Tris-saline (TS; pH7.6) and then a 30 min incubation in 0.5% BSA in TS. Sections then were incubated in primary chicken anti-GFP (1:3000) and mouse anti-GluN1 (1:50) for 24 hours at room temperature and 24 hours at 4°C. Sections then were incubated in goat anti-chicken biotinylated IgG (1:400; Jackson Immunoresearch Laboratories, West Grove, PA) for 30 min followed by a 30 min incubation in avidin-biotin complex (ABC; Vectastain Elite Kit, Vector Laboratories, Burlingame, CA) in TS (1:100 dilution). Sections were developed in 3,3′-diaminobenzidine (Sigma-Aldrich) and H_2O_2 in TS. All antibody incubations were performed in 0.1% BSA/TS and separated by washes in TS.

Sections next were processed for immunogold-silver detection of the mouse anti-GluN1 antibody using donkey anti-mouse IgG bound with 1 nm colloidal gold (1:50; Electron Microscopy Sciences, Fort Washington, PA; EMS) and incubated overnight at 4°C. Sections were fixed in 2% glutaraldehyde, and the gold particles were enhanced using a Silver IntenSEM kit (RPN491; GE Healthcare, Waukseka, WI) for 7 minutes.

Sections were post-fixed in 2% osmium tetroxide for 1 hr, dehydrated, and flat embedded in Embed-812 (EMS) between two sheets of Aclar plastic. Brain sections containing the PVN or RVLM were selected from the plastic embedded sections, glued onto Epon blocks and trimmed to 1mm-wide trapezoids. Ultrathin sections (70 nm thickness) through the tissue-plastic interface were cut with a diamond knife (EMS) on a Leica EM UC6 ultratome, and sections were collected on 400-mesh, thin-bar copper grids (EMS). Grids were then counterstained with uranyl acetate and Reynold's lead citrate.

Ultrastructural analysis

An investigator blinded to animal condition performed the data collection and analysis. The thin sections were examined and photographed on a CM10 transmission electron microscope (FEI, Hillsboro, OR). Cell profiles were identified by defined morphological criteria (Coleman et al., 2013; Peters et al., 1991). In particular, dendritic profiles generally were post-synaptic to axon terminals and contained regular microtubule arrays. Dendritic profiles were randomly sampled within each block. For each brain region in each animal, at least 50 dendrites were randomly selected and imaged from the plastic-tissue interface to ensure even antibody tissue penetration (Milner et al., 2011). Field selection criteria included clear

morphological preservation and the presence of immunolabeling. Immunoperoxidase labeling for GFP was evident as a characteristic, electron-dense DAB reaction product precipitate. Silver-intensified immunogold (SIG) labeling for GluN1 was visible as black, electron-dense particles. Profiles were considered labeled for immunogold-silver if they contained at least one SIG particle.

The subcellular localization of GluN1-SIG particles was defined as either on or near (within 70 nm, but not touching) the plasma membrane, or in the cytoplasm (Coleman et al., 2013; Marques-Lopes et al., 2014; Pierce et al., 2009). The presence of plasma membrane receptors (on PM) identified by SIGs corresponds to sites of receptor binding (Boudin et al., 1998; Ladepeche et al., 2014). The distribution of SIG labeled receptors shows the expected decrease in the ratio of surface-to-cytoplasmic localization in response to agonist stimulation (Haberstock-Debic et al., 2003). Therefore, it is likely that the distribution of protein as identified by SIGs reflects functional receptors. Receptors may be inserted into or removed from the plasma membrane from a pool of receptors near the plasma membrane (i.e., nrPM). Cytoplasmic receptors (cytoplasm) may be stored, in transit to/from the cell body or other cellular compartments, as well as in the process of receptor degradation or recycling (Fernandez-Monreal et al., 2012; Pierce et al., 2009).

Microcomputer Imaging Device software (MCID, Imaging Research Inc., Ontario, Canada) was used to determine the morphometry of single- and double-labeled dendrites; this included form factor, cross sectional perimeter, area, average diameter, and minor axis length (Coleman et al., 2013). Dendrites with an oblong or irregular shape, indicated by a form factor lower than 0.5, were excluded from the analysis.

The number, density, and partitioning ratio of SIG particles in each subcellular compartment and in all compartments (sum of SIG particles in all subcellular compartments) for each condition were statistically compared. The density of SIG particles is defined as the number of particles per cross sectional perimeter (per μm for on and near plasmalemmal compartments) or area (per μm^2 for cytoplasmic and all compartments). The partitioning ratio of SIG particles is defined as the number of SIG particles in a subcellular compartment as a proportion of the total number of SIG particles. Dendritic cross sectional perimeter, area, and average diameter also were compared across all groups.

Data analysis

Analysis of SBP measurements was conducted on days 9 or 10, time points associated with peak AngII-induced change in SBP in previous studies (Kawada et al., 2002). Since day-to-day conditions of the blood pressure measurements may differ, instead of using a repeated measures design and comparing to baseline, AngII SBP was compared to same-day Sal. Likewise, since males and females underwent pump implantations and SBP measurements in separate experiments at different times, t-tests were used to compare SBP in Sal vs. AngII in males and in females for the baseline measurement and a the post-implantation measurement.

In the RVLM, tissue from males and females were processed together for dual label immuno-EM, and thus between subject effects (i.e., male or female) and AngII

administration (i.e., saline or AngII) on GluN1 subcellular localization in RVLM CRF_1-containing dendrites were analyzed with a two-way ANOVA. Tukey HSD post-hoc tests were used to analyze significant main effects and interactions ($P < 0.05$).

In the PVN, tissue from males and females were processed separately for dual label immunohistochemistry for electron microscopy, and thus were analyzed separately for effects of AngII administration. While patterns of GluN1-SIG trafficking can be compared across immunoEM experiments, differences in antibody penetration preclude direct statistical comparisons of GluN1-SIG particles between males and females, and thus in the PVN, these data were analyzed by student's t-tests (saline vs. AngII) in males and females.

In our initial analysis, and in a recent paper (Marques-Lopes et al., 2015), AngII administration demonstrated significant sexually dimorphic effects on morphometric measures, such as average diameter. Thus, we examined the effect of AngII administration in both small (< 1.0 μm) and large (> 1.0 μm) dendrites within both the RVLM and PVN of male and female mice.

Data is presented as mean ± SEM. Analyses were considered statistically significant if $P < 0.05$. JMP8 (SAS Institute, Cary, NC) was used for statistical analyses.

Figure preparation

Images were cropped and final adjustments to brightness, contrast, and sharpness were made in Microsoft PowerPoint 2010. Graphs were generated using Prism 6 (GraphPad Software, La Jolla, CA).

RESULTS

CRF-EGFP neurons of the mouse RVLM and PVN contain tyrosine hydroxylase

Although several lines of evidence suggest that neurons expressing CRF_1 in the RVLM and PVN may have a role in blood pressure regulation (Justice et al., 2008; Ku et al., 1998; Milner et al., 1993; Yamaguchi et al., 2010), the expression of CRF_1 in cardiovascular-related neuronal phenotypes in these brain areas in the mouse is not known.

RVLM

By confocal microscopy, CRF_1-EGFP cells are observed throughout the RVLM (Fig. 1A1). The RVLM region harbors C1 catecholaminergic neurons that can be identified by the presence of TH, and the majority of TH containing neurons in the rostral portion of the RVLM project to the spinal cord (Guyenet et al., 2013; Phillips et al., 2001; Wang et al., 2006). Thus, we quantitatively examined these TH-containing RVLM neurons for CRF_1 co-labeling in 3 male mice. We found that 89.8 ± 3.8% of the neurons with CRF_1-EGFP immunoreactivity (ir) also contained TH-ir (Fig. 1A1–3) and 9.8% ± 3.6% contained only CRF_1-EGFP. Of neurons that contained immunolabeling for TH, 93.3 ± 3.0% also contained CRF_1-EGFP and 6.5 ± 3.0% contained only TH-ir. These findings indicate that a large majority of CRF_1-EGFP neurons in the sympathoexcitatory region of the RVLM are C1 neurons.

PVN

As a region of homeostatic integration and regulation, the PVN contains a diverse population of neurons (Benarroch, 2005), including segregated groupings of CRF and CRF_1 neurons (Justice et al., 2008). However, it is not known if CRF_1-containing PVN neurons project to the spinal cord, or contain markers (e.g., ERβ, AVP or TH) involved in cardiovascular regulation.

Consistent with previous studies (Justice et al., 2008), CRF_1-EGFP was prominent in mid-level sections (Bregma −0.80 mm) of the PVN (Fig. 1B1–E1). Following an injection of the retrograde tracer, fluorogold, into the thoracic spinal cord, CRF_1-GFP and fluorogold-labeled neurons had an overlapping distribution but were not colocalized (Fig. 1B1–3).

As previous studies have shown that the PVN contains ERβ and AVP expressing neurons that are involved in cardiovascular regulation (Biag et al., 2012; Coleman et al., 2013; Marques-Lopes et al., 2014), we next examined whether these proteins were co-expressed with CRF_1 in the PVN. Neither ERβ-ir (Fig. 1C1–3) nor AVP-ir (Fig. 1D1–3) were observed to colocalize with CRF_1-EGFP in PVN neurons.

TH-containing PVN neurons have been linked to the control of sympathetic outflow from the PVN (Shi et al., 2013). Thus, we examined whether TH was expressed in CRF_1-EGFP neurons in the PVN. We found that 89.8 ± 6.2% of neurons with CRF_1-EGFP also contained TH-ir and only 8.90 ± 5.37% contained only CRF_1-EGFP (Fig. 1E3). Of neurons with TH-ir, 82.6 ± 3.7% also contained CRF_1-EGFP and 15.7 ± 3.5% contained only TH-ir (Fig. 1E3). Thus, similar to the RVLM, the majority of CRF_1-EGFP neurons in the PVN colocalize TH; however, unlike the RVLM, CRF_1-EGFP neurons in the PVN do not project to the spinal cord.

Slow-pressor AngII increase systolic blood pressure in male but not in female mice

Prior to the implantation of osmotic mini-pumps, baseline blood pressure measurements in male and female CRF_1-EGFP mice were not significantly different. However, consistent with previous studies (Capone et al., 2012; Marques-Lopes et al., 2015; Marques-Lopes et al., 2014; Xue et al., 2007a), slow pressor AngII significantly increased SBP (measured at day 13 postimplant) in young adult males (peak mean systolic blood pressure + 22.0 ± 4.5 mmHg; t_{95}= 7.9; $P < 0.05$) but not in young adult females (t_{88} = 1.0; $P > 0.05$).

Sexual-dimorphism of GluN1 distribution in CRF_1-containing dendrites in the RVLM

The activation of sympathoexcitatory C1 neurons of the RVLM is critical to the increased blood pressure that occurs in response to AngII administration (Averill et al., 1994; Hirooka et al., 1997). In rats, these neurons respond to estradiol administration with an increase in the sensitivity of baroreceptor reflex, as well as a decrease in sympathetic output (Saleh et al., 2000). Moreover, AngII triggers larger Ca^{2+} currents in RVLM bulbospinal neurons in normal female compare to male rats (Wang et al., 2008). Given the importance of RVLM NMDA receptor activation in the regulation of blood pressure in spontaneously hypertensive rats (Lin et al., 1995; Lin et al., 2005; Zhang and Abdel-Rahman, 2002), and the finding that C1 neurons in the mouse contain CRF_1-EGFP, we used dual label immunoEM to determine

whether there were sex differences in the subcellular distribution of GluN1 in response to slow-pressor AngII administration in CRF_1-GFP-containing C1 neurons of young male and female mice.

Qualitative analysis—Qualitatively, within the RVLM, dendritic CRF_1-EGFP was characterized by diffuse immunoperoxidase reaction product (Fig. 2A–B). In contrast, GluN1-SIG particles were visualized as discrete electron dense black particles, which were often observed in dendritic profiles that also contained easily distinguishable peroxidase labeling for CRF_1-EGFP (Fig. 2A–B). Since over 80% of the CRF_1-EGFP neurons contained TH, a phenotype of many bulbospinal neurons in the RVLM (Guyenet et al., 2013), only dual-labeled dendrites containing both CRF_1-EGFP and GluN1-SIG particles were imaged and analyzed.

Subcellular distribution of GluN1 in the absence of AngII—The functional properties of receptors and other proteins are highly impacted by their subcellular location. The activation of NMDA receptors by extracellularly released ligand or exogenous drugs requires the presence of plasma membrane receptors (Boudin et al., 1998). We assessed the proportion of total SIG particles for GluN1 that were present on the plasma membrane, near the plasma membrane, or in the cytoplasm in dendritic profiles of RVLM neurons in male and female mice.

In the absence of AngII, there were significant sexual-dimorphisms in the partitioning ratio of GluN1 SIGs affiliated with distinct subcellular locations in CRF_1-EGFP dendritic profiles of RVLM neurons (Fig. 2C–D). The partitioning ratio is defined as the number of SIG particles in a subcellular compartment as a proportion of the total number of SIG particles. Females had a significantly higher plasma membrane GluN1 SIG partitioning ratio (t_{282} = −3.9, $P < 0.0001$), whereas males had a greater cytoplasmic GluN1 SIG partitioning ratio (t_{282} = 3.6, $P < 0.0005$). There were no differences in the partitioning ratio of near plasma membrane GluN1 SIGs in male and female mice (t_{282} = 4.7, $P > 0.1$).

Morphology in the absence of AngII—Alterations in dendritic and/or spine morphology have been correlated in hypertension (Sanchez et al., 2011; Vega et al., 2004) including in PVN-RVLM circuits (Sonner et al., 2008). Thus, the morphology of RVLM dendritic profiles was assessed in male and female mice. There were differences in the dendritic profile size of RVLM neurons expressing both GluN1 and CRF_1-EGFP labeling in male and female mice in the absence of AngII treatment (Fig. 2E–F). In male mice, the area (t_{282}= 4.7, $P < 0.0001$), average diameter (t_{282}= 4.6, $P < 0.0001$), and perimeter (t_{282}= 6.2, $P < 0.0001$) of CRF_1-EGFP dendritic profiles were greater than that of females.

Subcellular distribution of GluN1 following AngII administration—There were significant sex differences in the effects of AngII on the proportion of GluN1-SIG particles occurring on the plasma membrane. In male mice given AngII, the plasma membrane GluN1 SIG partitioning ratio was significantly higher compared to saline-treated animals (t_{304}= −2.0, $P < 0.05$; Fig. 2C). However, there was no difference in the plasma membrane GluN1 SIG partitioning ratio in CRF_1-EGFP dendrites in female mice receiving saline or AngII (t_{257}= 1.6, $P > 0.1$; Fig. 2D). There were no differences in the near plasma membrane (Male:

t_{304}= .29, P > 0 .7; Female: t_{257}= 0, P > 0.99) or cytoplasmic (Male: t_{304}= 0.9, P > 0.3; Female: t_{257}= 1.1, P > 0.2) GluN1 SIG partitioning ratio in CRF_1-EGFP dendrites in male or female mice treated with saline or AngII (Fig. 2C–D). There were also no differences in the density of GluN1 in CRF1-EGFP dendritic profiles in males (P > 0.05; Fig. 3A). However, the cytoplasmic density and total density of GluN1 particles in CRF1-EGFP dendrites was significantly increased in females (P < 0.05; Fig. 3B).

Proximal and distal dendritic compartments have been shown to have some degree of functional specialization in terms of signal conduction and synaptic plasticity (Froemke et al., 2005; Lovett-Barron et al., 2014). To assess the effect of AngII on the subcellular location of GluN1 in distinct functional dendritic compartments in the RVLM of male and female mice given AngII, CRF_1-EGFP dendrites were segregated into large (> 1.0 μm in diameter) and small (< 1.0 μm in diameter) sizes, presumably representative of proximal and distal dendrites within a single population. There was a significant effect of group (male vs. female) on the plasma membrane SIG partitioning ratio ($F_{1, 384}$ = 4.29; P < 0.02) in small, but not large dendrites (P > 0.05). Post-hoc analysis showed that male mice, but not female mice, given AngII compared to those given saline had a significantly increased plasma membrane GluN1 SIG partitioning ratio in small CRF_1-EGFP dendrites (P < 0.05, Fig. 3C,D).

Morphology following AngII—There were significant group (male vs female) differences in the dendritic morphology of male and female mice given AngII. In male mice, there were no differences in either the cross-sectional area (t_{304}= 1.7, P < 0.09), average diameter (t_{304}= 1.1, P > 0.2), or perimeter (t_{304}= 0.7, P > 0.4) of CRF_1-EGFP dendritic profiles when given either saline or AngII (Fig. 2E). However, in female mice given AngII, the cross-sectional area (t_{257}= −3.7, P < 0.0005) and perimeter (t_{257}= −3.7, P < 0.0005) of CRF_1-EGFP dendritic profiles were each higher than profiles in saline-treated animals (Fig. 2F).

Lack of sexual dimorphism in GluN1 localization in CRF1 dendrites of PVN neurons in the absence or presence of AngII

The presence of TH in CRF_1-containing PVN neurons suggests that CRF-sensitive neurons, which are known to contribute to sympathoexcitatory responses (Kang et al., 2011; Shi et al., 2013; Vacher et al., 2002), are also catecholaminergic. PVN dendrites lacking CRF_1-EGFP are derived from a heterogeneous population of neurons, including those containing angiotensin type 1 receptor (AT_1R) or ERβ (Gonzalez et al., 2012; Milner et al., 2010). Based on previous findings of sex differences in the partitioning of GluN1 in response to slow-pressor AngII in ERβ-containing PVN dendrites (Marques-Lopes et al., 2014), we analyzed GluN1-SIG particles in dendrites without CRF_1-EGFP. Tissue from males and females were processed separately for dual label immunoEM, and thus were analyzed separately.

Subcellular distribution of GluN1—In the PVN of both males and females, GluN1-SIG particles were evident in dendritic profiles also labeled for CRF_1-EGFP (Fig. 4A–B), as well as dendrites lacking CRF_1-EGFP immunoreactivity (Fig. 5A–B). In male or female mice

given saline or AngII, there were no significant differences ($P > 0.05$) in the plasma membrane, near plasma membrane or cytoplasmic GluN1 SIG partitioning ratio in dual labeled dendritic profiles (Fig. 4C–D), or dendrites showing exclusive GluN1 labeling (Fig. 5C–D) in the PVN.

In males, the density of GluN1-SIG particles was significantly greater in AngII-administered mice than in saline mice only in the cytoplasmic compartment of CRF_1-EGFP lacking dendritic profiles ($t_{355} = -2.5$; $P < 0.05$; Fig. 6A). AngII administration did not have a significant effect on the density of GluN1-SIG particles in any other subcellular compartment in single (Fig. 6A) and dual labeled (not shown) dendritic profiles of PVN neurons in male mice. In females, there was a significant effect of AngII administration on the density of near plasmalemmal GluN1-SIG particles ($t_{576.6} = 2.5$; $P < 0.05$; Fig. 6B), as well as the total density of GluN1 ($t_{559.4} = 2.0$; $P < 0.05$; Fig. 6B) in non-CRF_1-EGFP dendrites, with lower levels of GluN1 SIGs in AngII than in saline mice. There was no effect of AngII administration in any other subcellular compartments (Fig. 6B).

Morphology—In response to AngII, there was an increase in the area, average diameter, and perimeter of dual labeled dendritic profiles only in the PVN of female mice (Area: $t_{187.3} = -3.5$; Perimeter: $t_{223.3} = -3.6$; Average diameter: $t_{215.0} = -3.3$; $P < 0.05$; Fig. 4E–F). No morphological differences were seen in exclusive GluN1-labeled dendritic profiles in the PVN of male or female mice given saline or AngII (Fig. 5E–F).

DISCUSSION

Our ultrastructural studies demonstrate that in the absence of AngII, both the morphology and the distribution of GluN1 in CRF_1-containing dendrites of the RVLM differ in male and female mice. In addition, these studies also reveal that only males respond to a slow-pressor dose of AngII with both an increase in blood pressure and an elevation in the proportion of GluN1 on the plasma membrane of CRF_1-containing dendrites of neurons located in the RVLM, but not the PVN. These results highlight significant differences between males and females in both the pressor response and a differential plasticity of NMDA receptors in response to low dose AngII.

Sex differences in plasma membrane GluN1 in CRF_1-containing RVLM neurons following AngII administration

Following slow-pressor AngII-mediated hypertension there was an increase in the plasma membrane GluN1 SIG partitioning ratio in CRF_1-EGFP dendrites in RVLM neurons only in male mice. Furthermore, analysis of small (i.e., distal) and large (i.e. proximal) dendrites revealed that the significant effect of group (male vs female) on the GluN1 partitioning ratio was limited to small dendrites, which generally receive a higher number of excitatory type inputs (Froemke et al., 2005; Lovett-Barron et al., 2014). The increase in the relative distribution of GluN1 on the plasma membrane of CRF_1 expressing distal dendritic profiles contacted by glutamate inputs would suggest a hypertension-associated potentiation of NMDA receptor signaling in corticotrophin-sensitive RVLM neurons. This would be consistent with previous studies demonstrating the involvement of NMDA receptors in the

RVLM in pressor responses in spontaneously hypertensive rats (Lin et al., 1995; Lin et al., 2005; Zhang and Abdel-Rahman, 2002).

The RVLM is a critical regulator of the baroreflex arc by interfacing between first and second order mechanoreceptive inputs from the nucleus tractus solitarius and caudal ventrolateral medulla (Wehrwein and Joyner, 2013) and outputs to the spinal cord. The balance of excitation and inhibition in the RVLM in response to homeostatic stressors such as slow-pressor AngII administration is critical to maintaining blood pressure. The majority of rostral RVLM CRF_1-EGFP-containing neurons also express TH, suggesting that most of the CRF_1-GluN1 neurons are C1 bulbospinal neurons (Guyenet et al., 2013). In this context, the increased plasma membrane levels of GluN1 in RVLM neurons of males indicate that these neurons are in a potentiated state rendered more sensitive to excitation from glutamate inputs arising from other neural sites of blood pressure regulation like the PVN. Conversely, the relatively lower levels of GluN1 in females compared to males may favor increased baroreceptor sensitivity in females.

In rats, TH neurons in the RVLM express estrogen receptors (ERs) (Wang et al., 2006), and it is reasonable to hypothesize that the sex difference in the subcellular distribution of GluN1 in CRF_1-EGFP containing dendrites in the RVLM might involve sex hormone signaling. In ovariectomized rats, estradiol administration improves baroreceptor reflex sensitivity by decreasing sympathetic output as well as increasing parasympathetic tone (Saleh et al., 2000). In addition, ERβ is positioned within C1 bulbospinal neurons to modulate intracellular Ca^{2+} signaling in the RVLM (Wang et al., 2006). Moreover, ERα is present on axons terminals that contact C1 neurons where it may modulate transmitter release (Milner et al., 2008; Wang et al., 2006). Previous work from our group suggests that a sex difference in the subcellular distribution and levels of AT_1R, which is critical for reactive oxygen (ROS) production in the RVLM of rats (Pierce et al., 2009), may underlie the observed sex difference in ROS-dependent L-type Ca^{2+} currents in response to AngII in the RVLM (Wang et al., 2008). In sum, our findings suggest that substantial estrogen-mediated sex differences in glutamatergic and other signaling pathways in C1 neurons of the RVLM are likely. Therefore, conditions known to influence CRF release, like stress, may directly influence blood pressure regulation in a manner that differs in males and females. Our findings provide an anatomical basis for the influence of stress hormones and glutamate on neural regulation of blood pressure, and suggest that these CRF_1-expressing RVLM neurons may be sites of integration for stress-related and cardiovascular signals.

GluN1 repartitioning following AngII administration does not occur in CRF_1-GFP neurons of the PVN

The PVN critically integrates inputs from a variety of brain regions to coordinate various homeostatic processes, including blood pressure regulation and stress responses (Benarroch, 2005). Thus, the stability of GluN1 localization following AngII administration in PVN CRF_1-containing neurons suggests that plasticity in the subcellular location of NMDA receptors in this neuronal population likely is not involved in the response to slow pressor AngII in either males or females. However, it does not rule out a contribution of other

NMDA receptor-mediated signaling mechanisms in CRF_1-containing neurons in the response to hypertension.

The non-CRF_1-containing neurons in the PVN are neurochemically heterogeneous, and are likely to express CRF and AVP peptides (Coleman et al., 2013; Justice et al., 2008). These non-CRF_1-EGFP neurons in the PVN also likely contain ERβ or AT_1R (Marques-Lopes et al., 2015; Marques-Lopes et al., 2014). In agreement with the present studies, we found that near plasmalemmal GluR1 is elevated in PVN ERβ-EGFP neurons which are known to project to spinal cord (Marques-Lopes et al., 2014). The role of glutamate signaling in the sympathoexcitatory response to slow-pressor AngII administration in the mouse PVN in males has been previously demonstrated in a variety of these PVN neuronal populations, including those that are unlikely to express CRF_1 (Marques-Lopes et al., 2015; Marques-Lopes et al., 2014; Sonner et al., 2008; Wang et al., 2013). Notably, all of the studies to date in males have shown that slow pressor AngII elevates GluN1 in PVN neurons (Marques-Lopes et al., 2015; Marques-Lopes et al., 2014; Sonner et al., 2008; Wang et al., 2013). However, since changes in receptor location are significantly impacted by neurochemical phenotype, discrepancies between studies are likely to reflect sampling variance across diverse neuronal populations.

CONCLUSIONS

In contrast to the present results obtained from reproductively competent female mice, prior reports demonstrate that both ovariectomized female and aged female mice become hypertensive in response to slow pressor AngII (Marques-Lopes et al., 2014; Xue et al., 2007a; Xue et al., 2007b; Xue et al., 2013). The similar responses to AngII by both gonadally-deficient female and male mice, indicate that sexual dimorphisms in hypertension and associated brain plasticity involve gonadal hormone signaling. Therefore, the contrasting hypertension-associated NMDA receptor plasticity in CRF-sensitive neurons in the RVLM of males and females may provide an anatomical mechanism for gender-specific differences in the convergent modulation of RVLM neurons by stress hormones and glutamate. They also suggest that the relationship between stress and blood pressure regulation during the menopause transition warrants further investigation.

Acknowledgments

Supported by NIH grants HL098351and DA08259 (T.A.M.), HL096571 (C.I., V.M.P., M.J.G and T.A.M.), DA007274 (TAVK). We thank Ms. Sanoara Mazid for assistant with figure preparation.

ABBREVIATIONS

ABC	avidin-biotin complex
AngII	angiotensin II
AT_1R	angiotensin type 1 receptor
AVP	arginine vasopressin
BSA	bovine serum albumin

CRF	corticotropin releasing factor
CRF_1	corticotropin releasing factor type 1 receptor
Cy	cytoplasm
DAB	diaminobenzidine
EGFP	enhanced green fluorescent protein
EM	electron microscopy
ERβ	estrogen receptor beta
FG	fluorogold
GFP	green fluorescent protein
GluN1	NMDA glutamate receptor subunit 1
ir	immunoreactivity
onPM	on plasma membrane
NMDA receptor	N-methyl-D-aspartate receptor
PB	phosphate buffer
PM	plasma membrane
PVN	paraventricular nucleus of the hypothalamus
RVLM	rostral ventrolateral medulla
Sal	saline solution
SIG	silver-intensified gold
SBP	systolic blood pressure
TH	tyrosine hydroxylase
TS	Tris-saline

References

1. Appelman Y, van Rijn BB, Ten Haaf ME, Boersma E, Peters SA. Sex differences in cardiovascular risk factors and disease prevention. Atherosclerosis. 2015; 241:211–218. [PubMed: 25670232]
2. Averill DB, Tsuchihashi T, Khosla MC, Ferrario CM. Losartan, nonpeptide angiotensin II-type 1 (AT_1) receptor antagonist, attenuates pressor and sympathoexcitatory responses evoked by angiotensin II and L-glutamate in rostral ventrolateral medulla. Brain Res. 1994; 665:245–252. [PubMed: 7895060]
3. Beckerman MA, Van Kempen TA, Justice NJ, Milner TA, Glass MJ. Corticotropin-releasing factor in the mouse central nucleus of the amygdala: ultrastructural distribution in NMDA-NR1 receptor subunit expressing neurons as well as projection neurons to the bed nucleus of the stria terminalis. Exp Neurol. 2013; 239:120–132. [PubMed: 23063907]
4. Benarroch EE. Paraventricular nucleus, stress response, and cardiovascular disease. Clin Auton Res. 2005; 15:254–263. [PubMed: 16032381]
5. Biag J, Huang Y, Gou L, Hintiryan H, Askarinam A, Hahn JD, Toga AW, Dong HW. Cyto- and chemoarchitecture of the hypothalamic paraventricular nucleus in the C57BL/6J male mouse: a

study of immunostaining and multiple fluorescent tract tracing. J Comp Neurol. 2012; 520:6–33. [PubMed: 21674499]

6. Boudin H, Pélaprat D, Rostène W, Pickel VM, Beaudet A. Correlative ultrastructural distribution of neurotensin receptor proteins and binding sites in the rat substantia nigra. J Neurosci. 1998; 18:8473–8484. [PubMed: 9763490]
7. Brose N, Huntley GW, Stern-Bach Y, Sharma G, Morrison JH, Heinemann SF. Differential assembly of coexpressed glutamate receptor subunits in neurons of rat cerebral cortex. J Biol Chem. 1994; 269:16780–16784. [PubMed: 8207001]
8. Busnardo C, Alves FH, Crestani CC, Scopinho AA, Resstel LB, Correa FM. Paraventricular nucleus of the hypothalamus glutamate neurotransmission modulates autonomic, neuroendocrine and behavioral responses to acute restraint stress in rats. Eur Neuropsychopharmacol. 2013; 23:1611–1622. [PubMed: 23201369]
9. Capone C, Faraco G, Peterson JR, Coleman C, Anrather J, Milner TA, Pickel VM, Davisson RL, Iadecola C. Central cardiovascular circuits contribute to the neurovascular dysfunction in angiotensin II hypertension. J Neurosci. 2012; 32:4878–4886. [PubMed: 22492044]
10. Chan SH, Chan JY. Brain stem NOS and ROS in neural mechanisms of hypertension. Antioxid Redox Signal. 2014; 20:146–163. [PubMed: 23418728]
11. Cheng S, Xanthakis V, Sullivan LM, Vasan RS. Blood pressure tracking over the adult life course: patterns and correlates in the Framingham heart study. Hypertension. 2012; 60:1393–1399. [PubMed: 23108660]
12. Cohen BE, Edmondson D, Kronish IM. State of the Art Review: Depression, Stress, Anxiety, and Cardiovascular Disease. Am J Hypertens. 2015
13. Coleman CG, Wang G, Faraco G, Marques LJ, Waters EM, Milner TA, Iadecola C, Pickel VM. Membrane trafficking of NADPH oxidase p47(phox) in paraventricular hypothalamic neurons parallels local free radical production in angiotensin II slow-pressor hypertension. J Neurosci. 2013; 33:4308–4316. [PubMed: 23467347]
14. Coleman CG, Wang G, Park L, Anrather J, Delagrammatikas GJ, Chan J, Zhou J, Iadecola C, Pickel VM. Chronic intermittent hypoxia induces NMDA receptor-dependent plasticity and suppresses nitric oxide signaling in the mouse hypothalamic paraventricular nucleus. J Neurosci. 2010; 30:12103–12112. [PubMed: 20826673]
15. Creutz LM, Kritzer MF. Estrogen receptor-beta immunoreactivity in the midbrain of adult rats: regional, subregional, and cellular localization in the A10, A9, and A8 dopamine cell groups. J Comp Neurol. 2002; 446:288–300. [PubMed: 11932944]
16. Cuffee Y, Ogedegbe C, Williams NJ, Ogedegbe G, Schoenthaler A. Psychosocial risk factors for hypertension: an update of the literature. Curr Hypertens Rep. 2014; 16:483. [PubMed: 25139781]
17. Dimsdale JE. Psychological stress and cardiovascular disease. J Am Coll Cardiol. 2008; 51:1237–1246. [PubMed: 18371552]
18. Dingledine R, Borges K, Bowie D, Traynelis SF. The glutamate receptor ion channels. Pharmacol Rev. 1999; 51:7–61. [PubMed: 10049997]
19. Drouyer E, LeSauter J, Hernandez AL, Silver R. Specializations of gastrin-releasing peptide cells of the mouse suprachiasmatic nucleus. J Comp Neurol. 2010; 518:1249–1263. [PubMed: 20151358]
20. Fernandez-Monreal M, Brown TC, Royo M, Esteban JA. The balance between receptor recycling and trafficking toward lysosomes determines synaptic strength during long-term depression. J Neurosci. 2012; 32:13200–13205. [PubMed: 22993436]
21. Froemke RC, Poo MM, Dan Y. Spike-timing-dependent synaptic plasticity depends on dendritic location. Nature. 2005; 434:221–225. [PubMed: 15759002]
22. Fu Y, Neugebauer V. Differential mechanisms of CRF1 and CRF2 receptor functions in the amygdala in pain-related synaptic facilitation and behavior. J Neurosci. 2008; 28:3861–3876. [PubMed: 18400885]
23. Glass MJ, Hegarty DM, Oselkin M, Quimson L, South SM, Xu Q, Pickel VM, Inturrisi CE. Conditional deletion of the NMDA-NR1 receptor subunit gene in the central nucleus of the amygdala inhibits naloxone-induced conditioned place aversion in morphine-dependent mice. Exp Neurol. 2008; 213:57–70. [PubMed: 18614169]

24. Glass MJ, Robinson DC, Waters E, Pickel VM. Deletion of the NMDA-NR1 receptor subunit gene in the mouse nucleus accumbens attenuates apomorphine-induced dopamine D1 receptor trafficking and acoustic startle behavior. Synapse. 2013; 67:265–279. [PubMed: 23345061]
25. Glass MJ, Wang G, Coleman CG, Chan J, Ogorodnik E, Van Kempen TA, Milner TA, Butler SD, Young CN, Davisson RL, Iadecola C, Pickel VM. NMDA Receptor Plasticity in the Hypothalamic Paraventricular Nucleus Contributes to the Elevated Blood Pressure Produced by Angiotensin II. J Neurosci. 2015; 35:9558–9567. [PubMed: 26134639]
26. Goel N, Workman JL, Lee TT, Innala L, Viau V. Sex differences in the HPA axis. Compr Physiol. 2014; 4:1121–1155. [PubMed: 24944032]
27. Goncharuk VD, Van HJ, Swaab DF, Buijs RM. Paraventricular nucleus of the human hypothalamus in primary hypertension: activation of corticotropin-releasing hormone neurons. J Comp Neurol. 2002; 443:321–331. [PubMed: 11807841]
28. Gong S, Zheng C, Doughty ML, Losos K, Didkovsky N, Schambra UB, Nowak NJ, Joyner A, Leblanc G, Hatten ME, Heintz N. A gene expression atlas of the central nervous system based on bacterial artificial chromosomes. Nature. 2003; 425:917–925. [PubMed: 14586460]
29. Gonzalez AD, Wang G, Waters EM, Gonzales KL, Speth RC, Van Kempen TA, Marques-Lopes J, Young CN, Butler SD, Davisson RL, Iadecola C, Pickel VM, Pierce JP, Milner TA. Distribution of angiotensin type 1a receptor-containing cells in the brains of bacterial artificial chromosome transgenic mice. Neurosci. 2012; 226:489–509.
30. Guyenet PG, Stornetta RL, Bochorishvili G, Depuy SD, Burke PG, Abbott SB. C1 neurons: the body's EMTs. Am J Physiol Regul Integr Comp Physiol. 2013; 305:R187–R204. [PubMed: 23697799]
31. Haberstock-Debic H, Wein M, Barrot M, Colago EE, Rahman Z, Neve RL, Pickel VM, Nestler EJ, Von Zastrow M, Svingos AL. Morphine acutely regulates opioid receptor trafficking selectively in dendrites of nucleus accumbens neurons. J Neurosci. 2003; 23:4324–4332. [PubMed: 12764121]
32. Hart EC, Charkoudian N. Sympathetic neural regulation of blood pressure: influences of sex and aging. Physiology (Bethesda). 2014; 29:8–15. [PubMed: 24382867]
33. Hirooka Y, Potts PD, Dampney RA. Role of angiotensin II receptor subtypes in mediating the sympathoexcitatory effects of exogenous and endogenous angiotensin peptides in the rostral ventrolateral medulla of the rabbit. Brain Res. 1997; 772:107–114. [PubMed: 9406962]
34. Hof, PR.; Young, WG.; Bloom, FE.; Belichenko, PV.; Celio, MR. Comparative cytoarchitectonic atlas of the C57BL/6 and 129/SV mouse brains. Amsterdam: Elsevier; 2000.
35. Jinno S, Kosaka T. Immunocytochemical characterization of hippocamposeptal projecting GABAergic nonprincipal neurons in the mouse brain: a retrograde labeling study. Brain Res. 2002; 945:219–231. [PubMed: 12126884]
36. Justice NJ, Yuan ZF, Sawchenko PE, Vale W. Type 1 corticotropin-releasing factor receptor expression reported in BAC transgenic mice: implications for reconciling ligand-receptor mismatch in the central corticotropin-releasing factor system. J Comp Neurol. 2008; 511:479–496. [PubMed: 18853426]
37. Kagiyama S, Tsuchihashi T, Phillips MI, Abe I, Matsumura K, Fujishima M. Magnesium decreases arterial pressure and inhibits cardiovascular responses induced by N-methyl-D-aspartate and metabotropic glutamate receptors stimulation in rostral ventrolateral medulla. J Hypertens. 2001; 19:2213–2219. [PubMed: 11725166]
38. Kang YM, Zhang AQ, Zhao XF, Cardinale JP, Elks C, Cao XM, Zhang ZW, Francis J. Paraventricular nucleus corticotrophin releasing hormone contributes to sympathoexcitation via interaction with neurotransmitters in heart failure. Basic Res Cardiol. 2011; 106:473–483. [PubMed: 21287352]
39. Kaufling J, Veinante P, Pawlowski SA, Freund-Mercier MJ, Barrot M. Afferents to the GABAergic tail of the ventral tegmental area in the rat. J Comp Neurol. 2009; 513:597–621. [PubMed: 19235223]
40. Kawada N, Imai E, Karber A, Welch WJ, Wilcox CS. A mouse model of angiotensin II slow pressor response: role of oxidative stress. J Am Soc Nephrol. 2002; 13:2860–2868. [PubMed: 12444204]

41. Ku YH, Tan L, Li LS, Ding X. Role of corticotropin-releasing factor and substance P in pressor responses of nuclei controlling emotion and stress. Peptides. 1998; 19:677–682. [PubMed: 9622022]
42. Kubo T, Amano M, Asari T. N-methyl-D-aspartate receptors but not non-N-methyl-D-aspartate receptors mediate hypertension induced by carotid body chemoreceptor stimulation in the rostral ventrolateral medulla of the rat. Neurosci Lett. 1993; 164:113–116. [PubMed: 8152584]
43. Ladepeche L, Dupuis JP, Groc L. Surface trafficking of NMDA receptors: gathering from a partner to another. Semin Cell Dev Biol. 2014; 27:3–13. [PubMed: 24177014]
44. Lin JC, Tsao WL, Wang Y. Cardiovascular effects of NMDA in the RVLM of spontaneously hypertensive rats. Brain Res Bull. 1995; 37:289–294. [PubMed: 7627572]
45. Lin Y, Matsumura K, Kagiyama S, Fukuhara M, Fujii K, Iida M. Chronic administration of olmesartan attenuates the exaggerated pressor response to glutamate in the rostral ventrolateral medulla of SHR. Brain Res. 2005; 1058:161–166. [PubMed: 16143317]
46. Llewellyn-Smith IJ, Mueller PJ. Immunoreactivity for the NMDA NR1 subunit in bulbospinal catecholamine and serotonin neurons of rat ventral medulla. Auton Neurosci. 2013; 177:114–122. [PubMed: 23562375]
47. Lovett-Barron M, Kaifosh P, Kheirbek MA, Danielson N, Zaremba JD, Reardon TR, Turi GF, Hen R, Zemelman BV, Losonczy A. Dendritic inhibition in the hippocampus supports fear learning. Science. 2014; 343:857–863. [PubMed: 24558155]
48. Marques-Lopes J, Lynch MK, Van Kempen TA, Waters EM, Wang G, Iadecola C, Pickel VM, Milner TA. Female protection from slow-pressor effects of angiotensin II involves prevention of ROS production independent of NMDA receptor trafficking in hypothalamic neurons expressing angiotensin 1A receptors. Synapse. 2015; 69:148–165. [PubMed: 25559190]
49. Marques-Lopes J, Van KT, Waters EM, Pickel VM, Iadecola C, Milner TA. Slow-pressor angiotensin II hypertension and concomitant dendritic NMDA receptor trafficking in estrogen receptor beta-containing neurons of the mouse hypothalamic paraventricular nucleus are sex and age dependent. J Comp Neurol. 2014; 522:3075–3090. [PubMed: 24639345]
50. McEwen BS. Stress, sex, and neural adaptation to a changing environment: mechanisms of neuronal remodeling. Ann N Y Acad Sci. 2010; 1204(Suppl):E38–E59. [PubMed: 20840167]
51. Milner TA, Drake CT, Lessard A, Waters EM, Torres-Reveron A, Graustein B, Mitterling K, Frys K, Iadecola C. Angiotensin II-induced hypertension differentialy affects estrogen and progestin receptors are present in central autonomic regulatory areas of female rats. Exp Neurol. 2008; 212:393–406. [PubMed: 18533148]
52. Milner TA, Reis DJ, Pickel VM, Aicher SA, Giuliano R. Ultrastructural localization and afferent sources of corticotropin-releasing factor in the rat rostral ventrolateral medulla: Implications for central cardiovascular regulation. J Comp Neurol. 1993; 333:151–167. [PubMed: 7688383]
53. Milner TA, Thompson LI, Wang G, Kievits JA, Martin E, Zhou P, McEwen BS, Pfaff DW, Waters EM. Distribution of estrogen receptor beta containing cells in the brains of bacterial artificial chromosome transgenic mice. Brain Res. 2010; 1351:74–96. [PubMed: 20599828]
54. Milner, TA.; Waters, EM.; Robinson, DC.; Pierce, JP. Degenerating processes identified by electron microscpic immunocytochemical methods. In: Manfredi, G.; Kawamata, H., editors. Neurodegeneration, Methods and Protocols. New York: Springer; 2011. p. 23-59.
55. Noack HJ, Lewis DA. Antibodies directed against tyrosine hydroxylase differentially recognize noradrenergic axons in monkey neocortex. Brain Res. 1989; 500:313–324. [PubMed: 2575004]
56. Nunn N, Womack M, Dart C, Barrett-Jolley R. Function and pharmacology of spinally-projecting sympathetic pre-autonomic neurones in the paraventricular nucleus of the hypothalamus. Curr Neuropharmacol. 2011; 9:262–277. [PubMed: 22131936]
57. Perello M, Raingo J. Leptin activates oxytocin neurons of the hypothalamic paraventricular nucleus in both control and diet-induced obese rodents. PLoS ONE. 2013; 8:e59625. [PubMed: 23527232]
58. Peters, A.; Palay, SL.; Webster, Hd. The fine structure of the nervous system. 3. New York: Oxford University Press; 1991.
59. Petralia RS. Distribution of extrasynaptic NMDA receptors on neurons. Scientific World Journal. 2012; 2012:267120. [PubMed: 22654580]

60. Phillips JK, Goodchild AK, Dubey R, Sesiashvili E, Takeda M, Chalmers J, Pilowsky PM, Lipski J. Differential expression of catecholamine biosynthetic enzymes in the rat ventrolateral medulla. J Comp Neurol. 2001; 432:20–34. [PubMed: 11241375]
61. Pierce JP, Kievits J, Graustein B, Speth RC, Iadecola C, Milner TA. Sex differences in the subcellular distribution of angiotensin type 1 receptors and NADPH oxidase subunits in the dendrites of C1 neurons in the rat rostral ventrolateral medulla. Neuroscience. 2009; 163:329–338. [PubMed: 19501631]
62. Pierce JP, Kurucz O, Milner TA. The morphometry of a peptidergic transmitter system before and after seizure. I. Dynorphin B-like immunoreactivity in the hippocampal mossy fiber system. Hippocampus. 1999; 9:255–276. [PubMed: 10401641]
63. Polgar E, Thomson S, Maxwell DJ, Al-Khater K, Todd AJ. A population of large neurons in laminae III and IV of the rat spinal cord that have long dorsal dendrites and lack the neurokinin 1 receptor. Eur J Neurosci. 2007; 26:1587–1598. [PubMed: 17880393]
64. Prata J, Ramos S, Martins AQ, Rocha-Goncalves F, Coelho R. Women with coronary artery disease: do psychosocial factors contribute to a higher cardiovascular risk? Cardiol Rev. 2014; 22:25–29. [PubMed: 23867424]
65. Reckelhoff JF, Romero JC. Role of oxidative stress in angiotensin-induced hypertension. Am J Physiol Regul Integr Comp Physiol. 2003; 284:R893–R912. [PubMed: 12626356]
66. Reidman DA, Maher TJ, Chaiyakul P, Ally A. Modulation of extracellular glutamate and pressor response to muscle contraction during NMDA-receptor blockade in the rostral ventrolateral medulla. Neurosci Res. 2000; 36:147–156. [PubMed: 10711812]
67. Saleh TM, Connell BJ, Saleh MC. Acute injection of 17beta-estradiol enhances cardiovascular reflexes and autonomic tone in ovariectomized female rats [In Process Citation]. Auton Neurosci. 2000; 84:78–88. [PubMed: 11109992]
68. Sanchez F, Gomez-Villalobos MJ, Juarez I, Quevedo L, Flores G. Dendritic morphology of neurons in medial prefrontal cortex, hippocampus, and nucleus accumbens in adult SH rats. Synapse. 2011; 65:198–206. [PubMed: 20665725]
69. Sheng H, Zhang Y, Sun J, Gao L, Ma B, Lu J, Ni X. Corticotropin-releasing hormone (CRH) depresses n-methyl-D-aspartate receptor-mediated current in cultured rat hippocampal neurons via CRH receptor type 1. Endocrinology. 2008; 149:1389–1398. [PubMed: 18079206]
70. Shi YC, Lau J, Lin Z, Zhang H, Zhai L, Sperk G, Heilbronn R, Mietzsch M, Weger S, Huang XF, Enriquez RF, Baldock PA, Zhang L, Sainsbury A, Herzog H, Lin S. Arcuate NPY controls sympathetic output and BAT function via a relay of tyrosine hydroxylase neurons in the PVN. Cell Metab. 2013; 17:236–248. [PubMed: 23395170]
71. Shughrue PJ, Merchenthaler I. Distribution of estrogen receptor beta immunoreactivity in the rat central nervous system. J Comp Neurol. 2001; 436:64–81. [PubMed: 11413547]
72. Siegel SJ, Brose N, Janssen WG, Gasic GP, Jahn R, Heinemann SF, Morrison JH. Regional, cellular, and ultrastructural distribution of *N*-methyl-D-aspartate receptor subunit 1 in monkey hippocampus. Proc Natl Acad Sci USA. 1994; 91:564–568. [PubMed: 8290563]
73. Siegel SJ, Janssen WG, Tullai JW, Rogers SW, Moran T, Heinemann SF, Morrison JH. Distribution of the excitatory amino acid receptor subunits GluR2(4) in monkey hippocampus and colocalization with subunits GluR5-7 and NMDAR1. J Neurosci. 1995; 15:2707–2719. [PubMed: 7722624]
74. Smith GW, Aubry JM, Dellu F, Contarino A, Bilezikjian LM, Gold LH, Chen R, Marchuk Y, Hauser C, Bentley CA, Sawchenko PE, Koob GF, Vale W, Lee KF. Corticotropin releasing factor receptor 1-deficient mice display decreased anxiety, impaired stress response, and aberrant neuroendocrine development. Neuron. 1998; 20:1093–1102. [PubMed: 9655498]
75. Sonner PM, Filosa JA, Stern JE. Diminished A-type potassium current and altered firing properties in presympathetic PVN neurones in renovascular hypertensive rats. J Physiol. 2008; 586:1605–1622. [PubMed: 18238809]
76. Takemoto Y. The mapped pattern of kainate on blood pressure responses is similar to that of L-proline in the ventrolateral medulla of the rat. Neurosci Lett. 2007; 425:12–17. [PubMed: 17720316]
77. Turner, CD.; Bagnara, JT. General Endocrinology. Philadelphia: W.B. Saunders; 1971.

78. Vacher CM, Fretier P, Creminon C, Calas A, Hardin-Pouzet H. Activation by serotonin and noradrenaline of vasopressin and oxytocin expression in the mouse paraventricular and supraoptic nuclei. J Neurosci. 2002; 22:1513–1522. [PubMed: 11880481]

79. Valentino RJ, Bangasser D, Van Bockstaele EJ. Sex-biased stress signaling: the corticotropin-releasing factor receptor as a model. Mol Pharmacol. 2013; 83:737–745. [PubMed: 23239826]

80. Vega E, Gomez-Villalobos MJ, Flores G. Alteration in dendritic morphology of pyramidal neurons from the prefrontal cortex of rats with renovascular hypertension. Brain Res. 2004; 1021:112–118. [PubMed: 15328038]

81. Wang G, Coleman CG, Chan J, Faraco G, Marques-Lopes J, Milner TA, Guruju MR, Anrather J, Davisson RL, Iadecola C, Pickel VM. Angiotensin II slow-pressor hypertension enhances NMDA currents and NOX2-dependent superoxide production in hypothalamic paraventricular neurons. Am J Physiol Regul Integr Comp Physiol. 2013; 304:R1096–R1106. [PubMed: 23576605]

82. Wang G, Drake CT, Rozenblit M, Zhou P, Alves SE, Herrick SP, Hayashi S, Warrier S, Iadecola C, Milner TA. Evidence that estrogen directly and indirectly modulates C1 adrenergic bulbospinal neurons in the rostral ventrolateral medulla. Brain Res. 2006; 1094:163–178. [PubMed: 16696957]

83. Wang G, Milner TA, Speth RC, Gore AC, Wu D, Iadecola C, Pierce JP. Sex differences in angiotensin signaling in bulbospinal neurons in the rat rostral ventrolateral medulla. Am J Physiol Heart Circ Physiol. 2008; 295:R1149–R1157.

84. Wang J, Korczykowski M, Rao H, Fan Y, Pluta J, Gur RC, McEwen BS, Detre JA. Gender difference in neural response to psychological stress. Soc Cogn Affect Neurosci. 2007; 2:227–239. [PubMed: 17873968]

85. Wang WZ, Gao L, Wang HJ, Zucker IH, Wang W. Tonic glutamatergic input in the rostral ventrolateral medulla is increased in rats with chronic heart failure. Hypertension. 2009; 53:370–374. [PubMed: 19029485]

86. Weathington JM, Hamki A, Cooke BM. Sex- and region-specific pubertal maturation of the corticotropin-releasing factor receptor system in the rat. J Comp Neurol. 2014; 522:1284–1298. [PubMed: 24115088]

87. Wehrwein EA, Joyner MJ. Regulation of blood pressure by the arterial baroreflex and autonomic nervous system. Handb Clin Neurol. 2013; 117:89–102. [PubMed: 24095118]

88. Xue B, Johnson AK, Hay M. Sex differences in angiotensin II-induced hypertension. Braz J Med Biol Res. 2007a; 40:727–734. [PubMed: 17464437]

89. Xue B, Pamidimukkala J, Lubahn DB, Hay M. Estrogen receptor-alpha mediates estrogen protection from angiotensin II-induced hypertension in conscious female mice. Am J Physiol Heart Circ Physiol. 2007b; 292:H1770–H1776. [PubMed: 17142339]

90. Xue B, Zhang Z, Beltz TG, Johnson RF, Guo F, Hay M, Johnson AK. Estrogen receptor-beta in the paraventricular nucleus and rostroventrolateral medulla plays an essential protective role in aldosterone/salt-induced hypertension in female rats. Hypertension. 2013; 61:1255–1262. [PubMed: 23608653]

91. Yamaguchi N, Ogawa S, Okada S. Cyclooxygenase and nitric oxide synthase in the presympathetic neurons in the paraventricular hypothalamic nucleus are involved in restraint stress-induced sympathetic activation in rats. Neurosci. 2010; 170:773–781.

92. Zhang J, Abdel-Rahman AA. The hypotensive action of rilmenidine is dependent on functional N-methyl-D-aspartate receptor in the rostral ventrolateral medulla of conscious spontaneously hypertensive rats. J Pharmacol Exp Ther. 2002; 303:204–210. [PubMed: 12235252]

93. Zimmerman MC, Lazartigues E, Sharma RV, Davisson RL. Hypertension caused by angiotensin II infusion involves increased superoxide production in the central nervous system. Circ Res. 2004; 95:210–216. [PubMed: 15192025]

HIGHLIGHTS

2 CRF_1 neurons contain tyrosine hydroxylase in the RVLM and hypothalamus.

3 Slow pressor angiotensin II increases blood pressure in males but not females.

4 In males, AngII increases GluN1 on the plasmalemma of RVLM CRF_1 dendrites.

5 In females, AngII does not alter plasmalemmal GluR1 on RVLM CRF_1 dendrites.

6 In both sexes, AngII does not alter GluN1 localization in PVN CRF_1 dendrites.

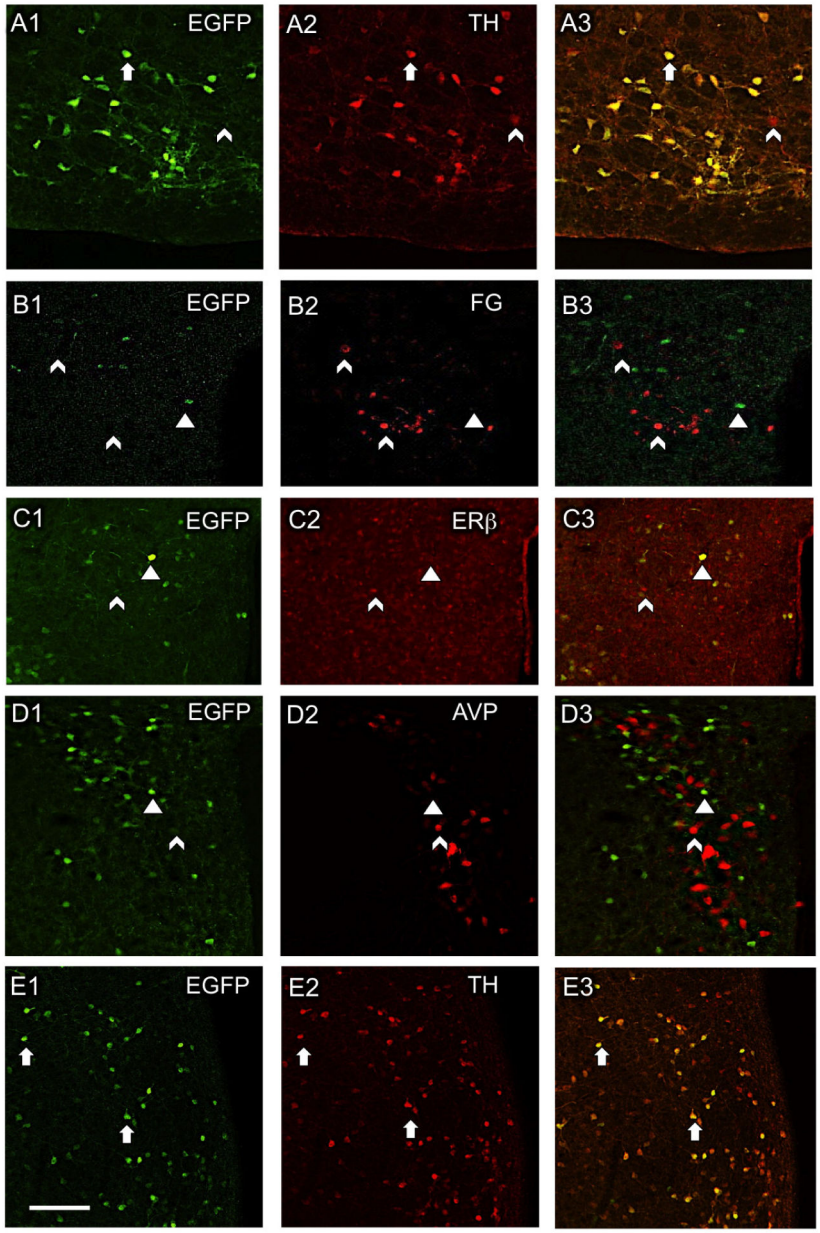

Figure 1. Distribution of CRF_1-EGFP relative to cardiovascular-related cellular phenotypes in the mouse RVLM and PVN

(A1–3) In the RVLM, most CRF_1-EGFP neurons contain TH. In the PVN, CRF_1-EGFP is not co-expressed with retrogradely transported fluorogold (FG) from the spinal cord **(B1–3)**, ERβ-ir **(C1–3)**, or AVP-ir **(D1–3). (E1–3)** Like the RVLM, most CRF_1-EGFP neurons in the PVN also contain TH. Arrows, colocalized labeling; arrowheads, CRF_1-EGFP only; chevron, Cy5 labeling only for non-CRF_1-EGFP markers. A, B, D and E = male mice; C = female mouse. Scale bar, 50 μm.

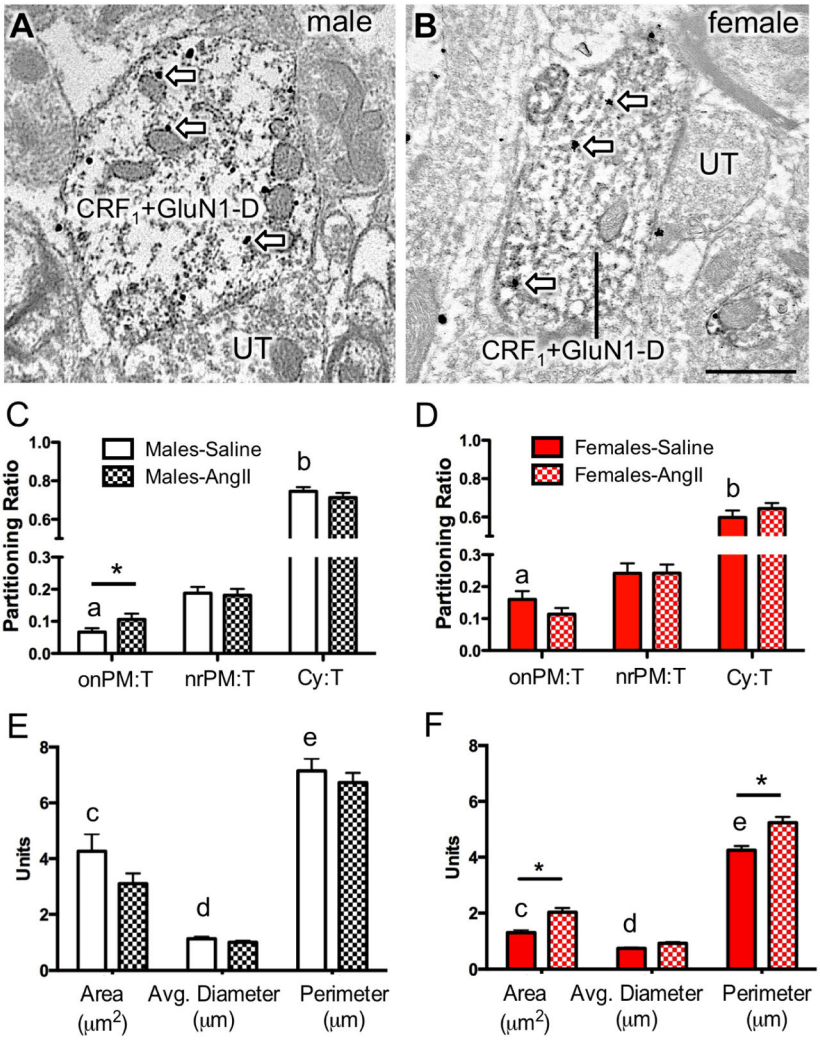

Figure 2. Dual GluN1 and CRF_1-EGFP containing dendrites of the RVLM in male and female mice administered saline or AngII: Subcellular distribution of GluN1 and dendritic morphology

(A, B) Representative images of dendrites from male **(A)** and female **(B)** mice containing both diffuse immunoperoxidase labeling for CRF_1-EGFP and black particulate labeling for GluN1 (arrows). **(C, D)** The partitioning ratio is shown as the number of SIG particles on the plasma membrane (onPM), near the plasma membrane (nrPM) or in the cytoplasm (Cy) relative to the total number of particles (T). In the absence of AngII, CRF_1-EGFP dendritic profiles from females show a significantly higher ratio of GluN1-SIG on the plasma membrane (onPM) compared to CRF_1-EGFP dendritic profiles from males. Following AngII, male mice show a significant increase in the ratio of onPM GluN1-SIG labeling. **(E, F)** In the absence of AngII, the area and the perimeter of CRF_1-EGFP containing dendrites is significantly larger in males compared to females. Following AngII, the area of CRF_1-EGFP dendritic profiles is significantly higher in AngII females compared to saline-treated females. *: $P < 0.05$ in saline versus AngII treated mice. a: $P < 0.05$ in female versus male mice given saline; b,c,d: $P < 0.05$ in male versus female mice given saline. UT, unlabeled terminal. Scale bar = 500 nm

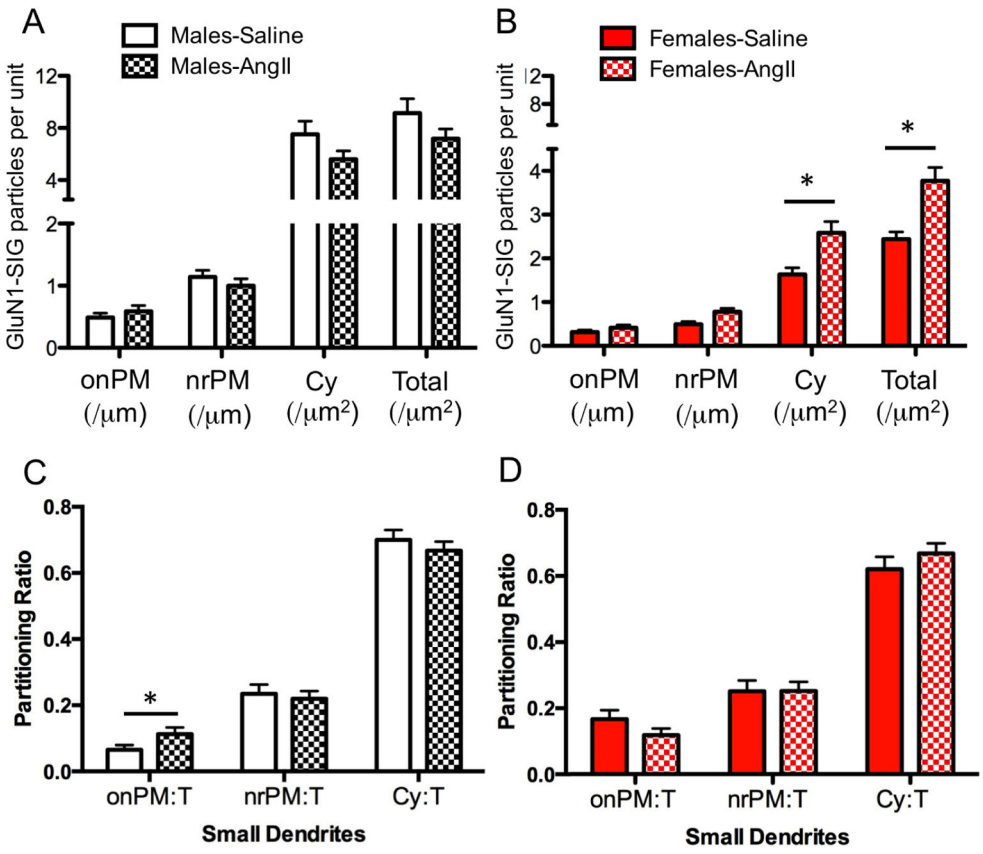

Figure 3. Dual GluN1 and CRF_1-EGFP containing dendrites of the RVLM in male and female mice administered saline or AngII: Density and partitioning ratio of GluN1

(A, B) The density of GluN1 labeling is shown as the number of SIG particles per dendrite. Labeling densities were calculated for on plasma membrane (onPM per μm), near plasma membrane (nrPM per μm), cytoplasm (Cyto per μm^2) or total (per μm^2). Cytoplasmic and total GluN1 density in CRF_1-EGFP dendrites was significantly greater in females **(B)** but not males **(A). (C,D)** The partitioning ratio is calculated as the number of GluN1 SIG particles in onPM, nrPM or cytoplasm divided by the total number of GluN1 SIG particles. Following AngII, the partitioning ratio of GluN1 SIGs is significantly increased in small CRF_1-EGFP dendrites (<1.0 μm in diameter) in males (**C**) but not females (**D**). *P < 0.05

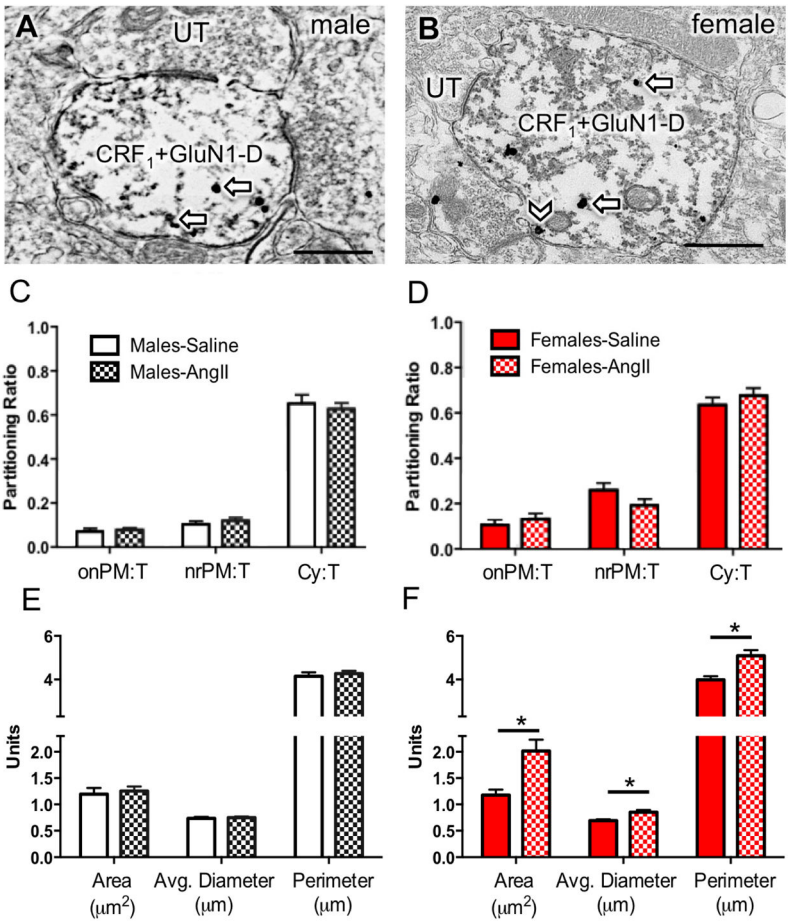

Figure 4. Dual GluN1 and CRF_1-EGFP containing dendrites from the PVN in male and female mice given saline or AngII: Subcellular distribution of GluN1 and dendritic morphology

(A, B) Representative images of dendrites from male **(A)** and female **(B)** mice showing both diffuse immunoperoxidase reaction product for CRF_1-EGFP and particulate labeling for GluN1 in the cytoplasm (arrows) or near the plasma membrane (chevron). **(C, D)** There is no difference in the partitioning ratio of GluN1 in male or female mice given saline or AngII. **(E, F)** The area, average diameter, and perimeter of dual GluN1 and CRF_1-EGFP containing dendrites is larger in males given AngII compared to males administered saline. *P < 0.05. UT, unlabeled terminal. Scale bar = 500 nm

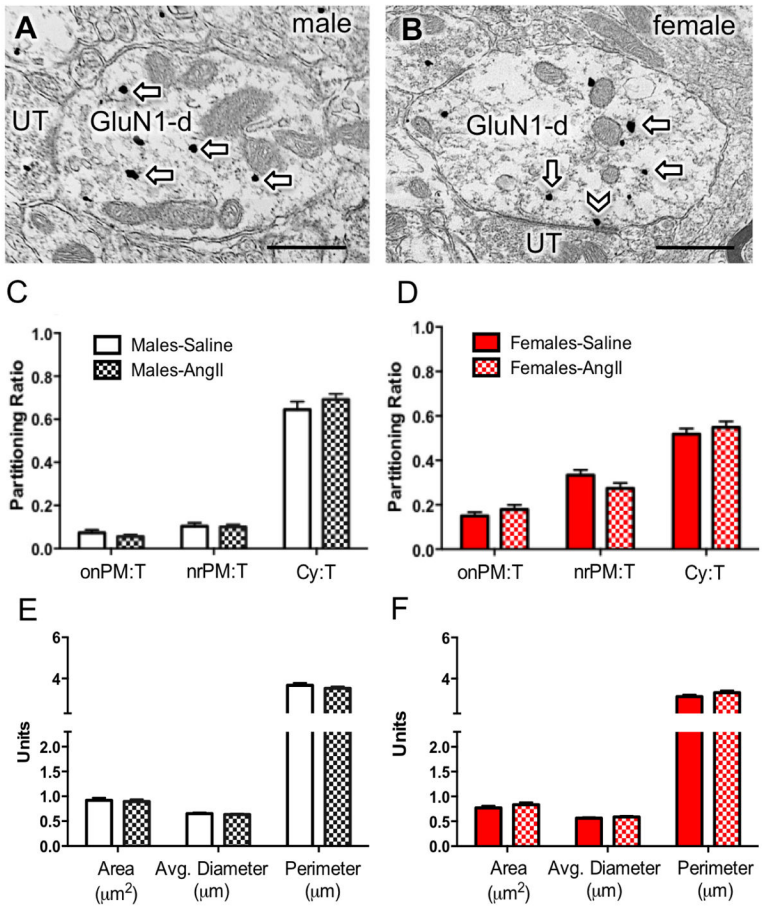

Figure 5. Dendrites containing only GluN1 from the PVN in male and female mice given saline or AngII: Subcellular distribution of GluN1 and dendritic morphology

Representative images of dendrites labeled with immunoperoxidase for CRF_1-EGFP (CRF_1-D) and immunogold-silver for GluN1 (black particles) in the cytoplasm (arrows) or near plasmalemma membrane (chevron) in the PVN of male **(A)** and female **(B)** mice. **(C, D)** The subcellular distribution of GluN1 SIG particles in dendrites is similar in males and females following saline or AngII. **(E, F)** There are no differences in the area, average diameter or perimeter of GluN1 dendrites following saline or AngII. UT, unlabeled terminal. *P < 0.05. Scale bar = 500 nm.

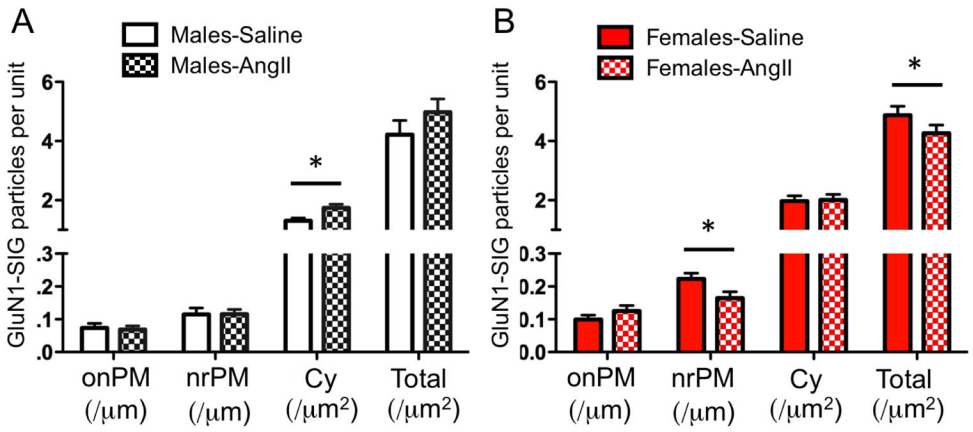

Figure 6. Dendrites containing only GluN1 from the PVN in male and female mice given saline or AngII: Density of GluN1 SIG particles

The density of GluN1 labeling is shown as the number of SIG particles per dendrite. Labeling densities were calculated for on plasma membrane (onPM per μm), near plasma membrane (nrPM per μm), cytoplasm (Cyto per μm^2) or total (per μm^2). Labeling density of GluN1 SIG for dendrites lacking CRF_1-EGFP **(A, B).** Following AngII, the density of GluN1 SIGs in non-CRF_1-EGFP dendrites significantly increased in the cytoplasm in males (**C**) but significantly decreased in the near plasma membrane and total in females (**D**). *P < 0.05